High-power laser-induced optical aberrations on beam director mirrors

Emine Yasemen Kaya Cekin,[a,*] **Yavuz Ozturk**,[b] **Eray Arpa**,[c] and **Aydin Yeniay**[a]

[a]TUBITAK-BILGEM, Electro-Optics and Laser Systems Group, Gebze, Turkey

[b]University of Cambridge, Electrical Engineering Division, Department of Engineering, Cambridge, United Kingdom

[c]TUBITAK-UZAY, Optical Systems Group, Ankara, Turkey

Abstract. We present a full-scale numerical study of thermally induced optical aberrations on the primary mirror of a beam director telescope. In particular, we investigate high-power laser-induced deformations, resulting monochromatic aberrations, and their effects on imaging and laser focusing performance of primary telescope mirrors in shared aperture beam director systems. As a practical example, we consider a system based on 6×4 kW single-mode high-power laser sources and a primary mirror having a 500 mm circular clear aperture. A detailed comparison of the monochromatic aberrations and their implications on the optical performance is provided for borosilicate and Zerodur® substrates having identical reflective coatings for potential laser beam director applications. Our analyses show that high-power lasers can be efficiently directed with negligible imaging degradation using athermal substrates (i.e., Zerodur®) with high reflective coatings (>99.9%) for primary mirrors. On the other hand, substrates with a relatively higher coefficient of thermal expansion (i.e., borosilicate) can only be used effectively under a strictly controlled ambient temperature. [DOI: 10.1117/1.OE.60.6.065102]

Keywords: high-power laser; directed energy systems; optical aberrations; high reflective mirror; Zernike polynomials; thermomechanical analysis.

Paper 20210286 received Mar. 16, 2021; accepted for publication May 24, 2021; published online Jun. 10, 2021.

1 Introduction

In recent years, high-power lasers (>kW) have become an enabling technology in many areas that include advanced material processing, lithography, and defense applications[1]. Both for industrial and defense applications, new generation competent systems having powers on the kW scale and beam qualities near the theoretical "single-mode Gaussian profile" limit have emerged with the advent of fiber lasers[2,3]. Advanced metal cutting–welding machines, 3D printers, and directed energy systems can be listed among the important contemporary applications. Although a great deal of effort has been invested in ever-increasing laser power, appropriate optics that can handle such laser powers still present some limitations. In regard to power handling of optical components, laser-induced damage threshold (LIDT) has been the main concern through the years and has inspired novel concepts in optical coating fabrications.[4–8] Today, LIDT remains a primary obstacle, and modern high-power lasers are utilized with expanded beam sizes; thus large optical apertures are needed to keep power density values below respective LIDT levels. On the other hand, although LIDT levels are critical in determining the catastrophic failure regime, laser-induced optical effects would start well below LIDT levels and may immensely impair laser system performance. To the best of our knowledge, such a mechanism and its effects on the optical systems have not been studied adequately. Hello and Vinet[9] reported analytic models of laser-induced thermal aberrations due to thermal lensing mechanism

*Address all correspondence to Emine Yasemen Kaya Cekin, yasemen.kaya@tubitak.gov.tr

0091-3286/2021/$28.00 © 2021 SPIE

(i.e., dn/dT). However, in their study, the effect of thermal expansion was excluded even though it is predominant for surface deformations of reflective optics and resulting optical aberrations. Since laser absorption takes place mainly in the first couple of layers of the high reflective mirror coating, surface deformations play a significant role in the calculation of optical aberrations, particularly if the thermal expansion coefficient of the substrate is large compared with that of the ultra-low expansion substrate. On the other hand, numerous prior analytical and numerical studies have been conducted for optical materials utilized in different systems from space/laser telescopes to LIGO input optics to analyze thermal effects caused by solar or relatively low-power laser exposures.[10–12] Furthermore, a particular component of spectral beam combining structure that potentially enables fiber laser power scaling has been investigated both numerically and experimentally in terms of laser-induced thermal deformation and effects on the combined beam properties.[13,14]

The study of high-power laser induced thermal effects, mechanical deformation, and, in turn, optical aberrations can provide a further understanding of the underlying physics along with the optimization of respective parameters to enhance the laser system performance. Therefore, it is imperative to study the influencing factors of high-power laser-induced thermal effects and the deformation of optical components under high-power laser exposure. High-power laser-induced optical aberrations can then be sorted out in terms of Zernike coefficients, and their effects on system performance (i.e., imaging and laser focusing performance for a primary telescope mirror) can easily be computed.

In general, laser systems depend on either refractive (lenses) and/or reflective (mirrors) in manipulating the beam. In the case of mirrors, multistack dielectric coatings are commonly preferred. Various dielectric coating technologies can be utilized for a specific laser emission spectrum.[15] It is clear that, for demanding high-power laser applications, a high reflectivity (i.e., $>99.9\%$), a low absorption rate, and a high coating uniformity with a defect-free process are among key parameters for minimizing undesired laser absorption that causes surface deformations and potential catastrophic failure. The optical coatings used in highly reflective mirrors are commonly composed of alternating multiple dielectric layers to provide low-light absorption and high reflectance for a certain wavelength range. The surface quality of the coatings depends on the deposition method such as ion beam sputtering, plasma vapor deposition, and magnetron sputtering.[16] Although these mirrors provide reflection over 99.9%, the amount of energy that they absorb when exposed to high-power laser beams can still inflict significant surface deformation. Thermomechanical properties of the substrate material play a key role in the deformations and the resulting optical aberrations. For such challenging applications, ultra-low expansion (i.e., ULE®, Zerodur®, Astrosital®, and Clearceram®) materials having thermal expansion coefficients as low as 10^{-9} to 10^{-8} $1/\mathrm{K}$ at temperatures 23°C to 35°C are commonly preferred as the mirror substrates.[17,18] Such substrates also enable optical systems to operate over a wide temperature range with little or negligible performance degradation under harsh environmental conditions (i.e., day-night cycles or space-born applications).

For some laser applications in which the exposure takes place on the order of minutes if not seconds, ordinary materials such as fused silica and borosilicate can also be of interest as high-performance coatings may provide adequate immunity from the exposure. Borosilicate, a lightweight structure with a thermal expansion coefficient of 3.25×10^{-6} $1/\mathrm{K}$, can be a good cost-effective alternative to ultra-low expansion materials as it can easily be molded owing to its low melting temperature and malleable nature. Its low mass density can also provide mechanical advantages, especially for large diameter telescope mirrors in which the weight and overall natural frequency of the system would be dramatically improved.

In this study, we investigate high-power laser-induced optical aberrations on a primary telescope mirror and their effects on the imaging and the laser focusing performance of a shared aperture beam director system. Laser power absorbed by the mirror surface induces surface deformations due to thermal expansion, resulting in various monochromatic aberrations. In our study, conformal mirror surface deformations and resulting aberrations as well as their effects on telescope performance in terms of laser spot size and MTF were analyzed via computing the respective coefficients of the Zernike polynomials. We considered a practical system that utilizes high-power laser sources and a primary mirror of 0.5-m diameter. A detailed comparison of the optical aberrations and their implications on the performance is provided for borosilicate and

Zerodur® substrates having identical reflective coatings under similar high-power laser exposure for potential laser beam director applications. Our analyses show that high-power lasers can be efficiently directed with negligible imaging degradation if low expansion substrates (i.e., Zerodur®) with high reflective coatings ($> 99.9\%$) are utilized for primary mirrors. On the other hand, despite having a much higher coefficient of thermal expansion compared with those of low expansion substrates, a low-cost material, borosilicate, can also be utilized as a high-power laser mirror substrate under certain ambient temperature ranges provided a high reflective coating is employed.

A Ritchey–Chrétien (RC) telescope was studied here since the base aberrations for it are already minimal; thus contribution from high-power laser-induced thermal load could be the dominant factor. On the other hand, cost effective and easy to align director configurations such as Dall-Kirkham designs may also provide a viable solution in comparison with those of RC telescope designs in practical applications, in which atmospheric effects, tracking errors, and laser beam quality factors would generally determine the overall performance limitations.

Another interesting aspect of this study is the numerical model developed to analyze a shared aperture laser beam director system. We constructed an extensive mathematical model to calculate the optical aberrations caused by the thermal expansion of a conical mirror due to high-power laser exposure. The conical mirror analyzed here is the primary mirror (M1) of a RC type telescope system. The numerical analyses were performed in four steps for the two materials Zerodur®[19] and Borofloat® 33[20,21] (Schott) in which the M1 substrate can be cast; then the results were compared. First, an electromagnetic analysis was performed in a time-harmonic form to calculate the amount of electromagnetic energy transformed into thermal energy on the mirror surface (in the coating). The ratio between the absorbed power and the incident power was utilized as the absorptivity of the mirror in the thermomechanical analysis. In the second step, six beams arranged in a honeycomb geometry, each having 4k laser power, were applied on the mirror surface simultaneously and modeled as individual heat sources with each having a Gaussian profile. Surface deformations in all three dimensions due to the laser heating together with the force of gravity were computed by time-dependent finite-element analysis (FEA). The anisotropic (multilayer) structure of the coating was taken into account and modeled as a composite material. In the third step, the optical aberrations caused by the surface deformations were analyzed by means of the Zernike polynomials. The deformed surface sag calculated in the thermomechanical analysis was fitted into Zernike polynomials and coefficients were computed in MATLAB by the least squares method. Finally, the Zernike coefficients of the deformed surfaces were imported into Zemax, and the spot size and MTF analyses were carried out to study the optical performances of the telescope systems.

2 Mathematical Model

2.1 *Electromagnetic Analysis (FEM)*

We analyzed a high reflective conical mirror with a faceplate of 1-cm thickness and a dielectric coating on top that consists of 15 alternating Ta_2O_5/SiO_2 layers, each having equal optical thickness (quarter-wave):

$$nt = \lambda/4,$$

where n and t are the real part of the refractive indices and thickness of the corresponding material, respectively, both at the laser wavelength λ (Fig. 1). The RMS value of surface roughness was assumed to be 5 nm in the model.

High reflective dielectric coatings rely on the interference of light from the layers of the periodic medium. In the case of a quarter-wave stack, reflected waves at the interfaces add constructively since the optical thickness of the period at the particular wavelength is half wave. This leads to the maximum reflectance of the coating, which increases as more layers are added to the stack. However, in spite of the coating, not all of the light that falls on the mirror can be reflected. Some of the light that is transmitted and reflected within those layers is absorbed, depending on the extinction coefficient κ of the corresponding material. Due to Ta_2O_5 layers having a

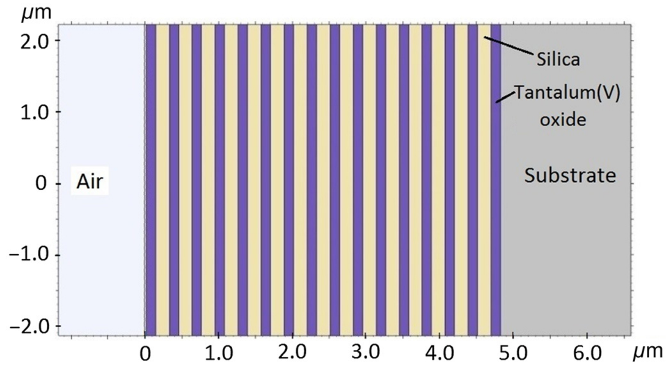

Fig. 1 Optical parameters (see Refs. 22–24) and the geometry of the coating cross section utilized in the electromagnetic analysis (wavelength $\lambda = 1075$ nm).

relatively high extinction coefficient, we expect laser light to be absorbed mainly within those layers, i.e., inside the coating.

To model each laser beam in the thermomechanical model, we first need to know how much light is absorbed within the mirror, i.e., the amount of electromagnetic energy transferred into thermal energy inside the mirror. Therefore, considering a cross section (zy plane) of the mirror parallel to the mirror axis, we solved the following 2D wave equation in time harmonic form:

$$\nabla \times (\nabla \times E) - k_0^2 \varepsilon_r E = 0, \quad E(x, y, z) = \tilde{E}(y, z) e^{-ik_x x}, \tag{1}$$

where E is the electric field, k_0 is the wave number in vacuum, and $\varepsilon_r = (n - i\kappa)^2$ is the relative permittivity. With an out of plane polarization assumption (x axis $k_x = 0$), dissipation (electromagnetic power loss) was calculated through the layers of the mirror, and the proportion of the power loss was defined to be the absorptivity A of the mirror. The calculations showed that almost all of the dissipated power is absorbed in the coating (≈ 5 μm), which allowed us to consider the laser beams in the thermomechanical model to be boundary heat sources acting on the front surface.

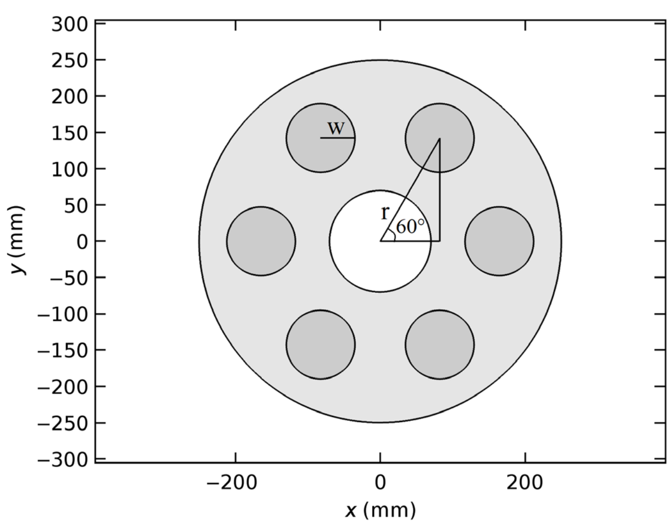

Fig. 2 Hexagonal configuration of the laser beam heat sources that primary mirror surface was exposed to. Circumradius is $r = 164$ mm, and beam spot radius on the mirror surface is $w = 47$ mm ($1/e2$ half width).

2.2 *Thermomechanical Analysis (FEM)*

In high-power laser systems, power scalability can be achieved by utilizing multiple laser sources since the maximum available single laser power (i.e., 5 to 10 kW) has technological limits. Therefore, in this model, we consider six beams arranged in a honeycomb geometry, each having 4 kW laser power, applied on the mirror simultaneously (Fig. 2). Laser output beam sizes are generally determined by optimizing spot size and MTF by taking into account the diffraction and atmospheric effects (e.g., $r0$, Fried parameter). In normal atmospheric conditions, (i.e., $Cn^2 \sim 10^{-14}\ \mathrm{m}^{-\frac{2}{3}}$), the ideal output beam size is to be on the order of 140 mm (Fried parameter, $r0 \sim 70$ mm) in diameter.[25] As multiple laser sources are utilized for the sake of power scalability, overall size of the primary mirror should be large enough to cover all laser beams. The conical primary mirror analyzed in this model has a lightweight structure with an open-back configuration, and its thickness-to-diameter ratio is 1:10. It is an annular mirror with a 140 mm inner diameter and 500 mm circular clear aperture. The effective size (diameter) of each laser beam on the mirror is 94 mm at $1/e^2$ full width (~143 mm at 99% full width) as depicted in Fig. 2.

As the first step of the thermal calculations, a steady-state mechanical analysis was performed to compute the sag deformations due to gravity. In the second step, the mirror exposed to the six laser beams for 30 s was studied by carrying out a time-dependent fully coupled thermomechanical analysis to compute the sag deformations caused by the laser heating.

The six laser beams in the model were considered to be centered at the corners of a regular hexagon with a circum radius r (see Fig. 2). The absorbed power due to each laser beam was calculated by multiplying the surface absorptivity and the incident beam power. The laser irradiance of each beam was defined by a Gaussian distribution. Therefore, the total laser irradiance on the mirror surface is written as the following sum of six individual Gaussian beams each centered at (a_i, b_i):

$$-n \cdot (-k\nabla T) = AP\frac{2}{\pi w^2}\sum_{i=1}^{6} e^{-\frac{2((x-a_i)^2+(y-b_i)^2)}{w^2}}, \tag{2}$$

where k is the thermal conductivity, T is the temperature, A is the absorptivity, P is the beam power, and w is the beam spot radius measured on the mirror surface ($1/e^2$ half width).

Inside the domain, a coupled system of partial differential equations describing the deformation of the mirror due to laser heating is solved. The coupling is between the heat transfer and the solid mechanics; thus the thermal expansion was implemented via the thermal strain tensor $\epsilon_{\mathrm{th}} = \alpha(T - T_0)$,

heat equation:

$$\rho C_p \dot{T} + \nabla(-k\nabla T) = 0, \tag{3}$$

equations of motion:

$$\begin{cases} \rho\ddot{\boldsymbol{u}} - \nabla\sigma = \rho g, \sigma = \boldsymbol{C}:(\epsilon - \epsilon_{\mathrm{th}}), \\ \epsilon = \frac{1}{2}[(\nabla\boldsymbol{u})^{\mathrm{T}} + \nabla\boldsymbol{u}], \epsilon_{\mathrm{th}} = \alpha(T - T_0), \\ \boldsymbol{C} = \boldsymbol{C}(E, \nu, G), \end{cases} \tag{4}$$

where ρ is the density, C_p is the heat capacity, $\boldsymbol{u}$ is the displacement field, g is the acceleration of gravity, σ is the Cauchy stress tensor, ϵ is the strain tensor, ϵ_{th} is the thermal strain tensor, α is the thermal expansion coefficient, T_0 is the ambient (and reference) temperature, C is the elasticity tensor, E is the Young's modulus, ν is the Poisson's ratio, and G is the shear modulus.

Convective and radiative heat flux boundary conditions were applied on the outer surfaces of the mirror:

$$-n \cdot (-k\nabla T) = h(T_0 - T) + \varepsilon\sigma_1(T_0^4 - T^4), \tag{5}$$

where h is the heat transfer coefficient, ε is the emissivity of the surface, and σ_1 is the Stefan–Boltzmann constant.

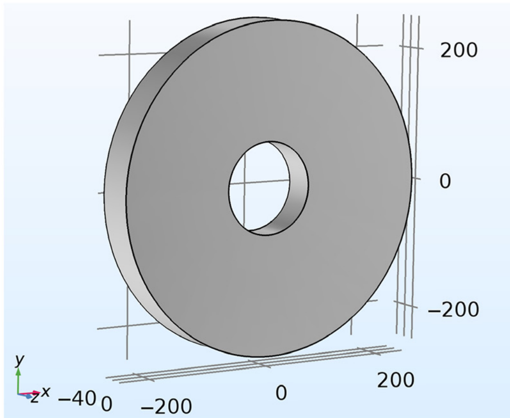

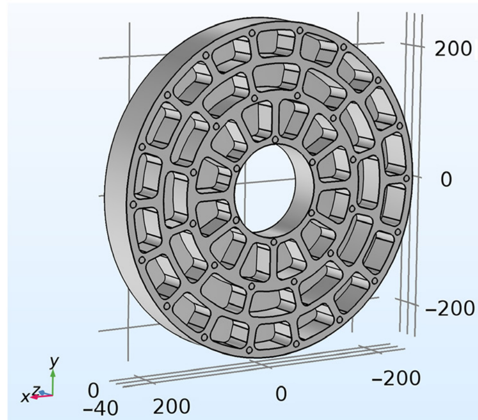

Fig. 3 Geometry (in mm) of the mirror utilized in the thermomechanical analysis: (a) front view and (b) back view with the circular spots where the mirror is assumed to be fixed.

The 36 circular spots on the back of the mirror—each having 10 mm diameter—[Fig. 3(b)] were considered fixed boundaries:

$$u = 0. \tag{6}$$

All other boundaries were taken to be free:

$$\sigma \cdot n = 0. \tag{7}$$

In this model, initial, ambient, and reference temperatures were considered to be $T_0 = 20°\mathrm{C}$, and the convective cooling was taken into account with a heat transfer coefficient $h = 5\ \mathrm{W}/(\mathrm{m}^2\,\mathrm{K})$.

The fixed boundary assumption of the 36 spots can be justified as follows. In practice, the mirror is fastened with an adhesive, the stiffness of which plays a role in the deformation of the mirror and therefore the optical performance of the telescope. In particular, when the ambient temperature is not controlled, the thermal expansion/contraction of the adhesive as well as that of the mechanical components holding the optics should be taken into account in the thermomechanical model. However, since the ambient temperature was considered to be 20°C in the current analyses, it is a reasonable assumption and simplification of the mechanical model to consider the boundaries simply fixed. In addition, the location and size of these spots can be further optimized to reduce the surface deformation and the resulting optical aberrations.[26]

The anisotropic nature of the multilayered coating structure was taken into account by means of implementing—analytically calculated—effective material properties into the thermomechanical model, and it was modeled as a composite material on top of the substrate material.[27,28] Material properties of the coating together with the substrates that were utilized in the thermomechanical model are presented in Table 1.

As mentioned, Zerodur is commonly used as a low-thermal expansion glass ceramic material. It is a material with a low CTE on the order of 10^{-8} 1/K over a wide temperature range and approaching zero around 320 K (Fig. 4). Zerodur also exhibits excellent homogeneity of this coefficient throughout the entire large bulk material, which makes it an ideal mirror substrate in cases requiring extreme thermal stability. On the other hand, borosilicate, being one of the most common materials used for both reflective and transitive IR optics, has a relatively larger CTE in comparison with that of Zerodur (Fig. 4). However, it is well known for its thermal shock resistance and cost-effective straightforward manufacturability. In addition, borosilicate can easily be molded into (thermally shaped) lightweight structures with improved cooling properties, making it easier to produce enlarged back surfaces for large optics.[30]

Table 1 Physical parameters of the substrate materials Zerodur and borosilicate; coating materials Ta_2O_5/SiO_2 and the composite structure of the coating with 15 pairs of Ta_2O_5/SiO_2 used in the thermomechanical analysis.[29] Thermal expansion coefficient of Zerodur is a temperature-dependent continuous function as plotted in Fig. 4.

	Substrate		High-index layer	Low-index layer	Coating (Ta_2O_5/SiO_2)	
	Zerodur®	Borofloat® 33	Ta_2O_5	SiO_2	Along layers (effective ∥)	Normal to layers (effective ⊥)
k (thermal conductivity), W/(mK)	1.46	1.2	33	1.38	14.8	2.3
C (heat capacity), J/(kg K)	800	830	308.8	703	428.7	
ρ (density), kg/m^3	2530	2200	6800	2203k	4143	
α (thermal expansion coefficient), 1/K	-2.4×10^{-8} at 20°C	3.25×10^{-6}	3.6×10^{-6}	0.55×10^{-6}	2.34×10^{-6}	2.14×10^{-6}
E (Young's modulus), GPa	90.3	64	140	73.1	101.2	92.3
G (shear modulus), GPa	36.4	26.7	56.9	31.2	$G_{L\perp} = 38.8$ $G_{LL} = 42.0$	
ν (Poisson's ratio)	0.24	0.2	0.23	0.17	0.195	0.177
ε (emissivity)	0.9	0.9			0.9	

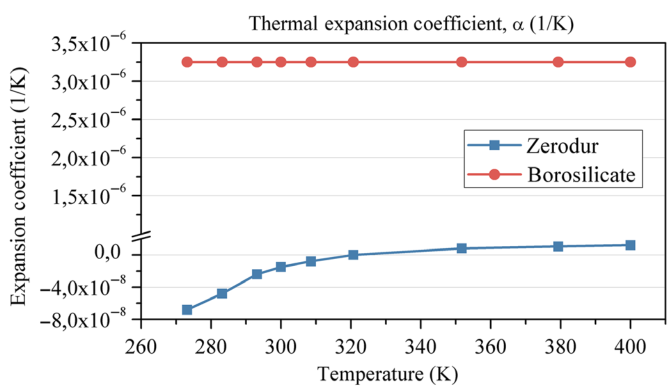

Fig. 4 Thermal expansion coefficients of the substrate materials utilized in the thermomechanical models.

2.3 *Optical Analysis/Zernike Polynomials Fit (MATLAB and Zemax)*

The optical aberrations of the deformed mirror surface were analyzed in terms of Zernike annular polynomials, which form a complete set of orthonormal polynomials over an annular region. These polynomials are used to fit the sag deformations as perturbations to the mirror surface:

$$\tilde{s}(r,\theta) = s(r,\theta) + \sum_{n=0}^{M} \sum_{m=-n}^{n} c_{nm} Z_n^m(r,\theta,\epsilon), \tag{8}$$

where s and $\tilde{s}$ represent the sag of the undeformed and deformed configurations, respectively; c_{nm} are the coefficients of the orthonormal Zernike annular polynomials $Z_n^m(r,\theta,\epsilon)$; and ϵ is the obscuration ratio of the annular pupil. In our model, the undeformed mirror (base surface) s is a conic surface with a conic constant κ and curvature c and is defined as

$$s(r,\theta) = s(r) = \frac{cr^2}{1 + \sqrt{1 - (1+\kappa)c^2 r^2}}. \tag{9}$$

Zernike annular polynomials (see Table 2) are obtained from Zernike circular polynomials using the Gram–Schmidt orthogonalization process,[31] and they are orthonormal in the following sense:

$$\int_\epsilon^1 \int_0^{2\pi} Z_n^m(r,\theta,\epsilon) Z_{n'}^{m'}(r,\theta,\epsilon) r\mathrm{d}r\,\mathrm{d}\theta \Big/ \int_\epsilon^1 \int_0^{2\pi} r\mathrm{d}r\,\mathrm{d}\theta = \delta_{nn'}\delta_{mm'} \tag{10}$$

where δ_{ij} is the Kronecker delta.

To fit the sag deformation data into Zernike polynomials, we implemented the finite-element displacements obtained in the thermomechanical analyses into MATLAB. However, it has been pointed out by Doyle[32] that the sag deformation is not equal to the finite-element computed z-displacement if the node position is also displaced in the radial direction. Therefore, the changes in the sag were approximated by Doyle in the following way:

$$\begin{aligned}\Delta s(r_0,\theta_0) &= \tilde{s}(r_0,\theta_0) - s(r_0) \\ &= w(r_0,\theta_0) - \frac{\partial s(r_0)}{\partial r}\sqrt{u^2(r_0,\theta_0) + v^2(r_0,\theta_0)},\end{aligned} \tag{11}$$

where $\langle u, v, w\rangle$ is the node displacement field of the mirror surface in rectangular coordinates. This formula provides the sag deformation of the finite-element node at the undeformed radial position (r_0,θ_0). We, on the other hand, propose a formulation that more conveniently provides the deformation of the sag at the displaced radial position of the node. The sag change of the mirror at the displaced radial position $(\tilde{r},\tilde{\theta})$ is formulated in the following way (Fig. 5):

$$\Delta s(\tilde{r},\tilde{\theta}) = \tilde{s}(\tilde{r},\tilde{\theta}) - s(\tilde{r}) = w(r_0,\theta_0) - [s(\tilde{r}) - s(r_0)], \tag{12}$$

where $\tilde{r} = r_0 + \sqrt{u^2 + v^2}$.

Table 2 Annular Zernike polynomials for primary aberrations as is given in Zemax.

Aberration name	#	n	m	Zernike polynomial $Z_n^m(r,\theta,\epsilon)$
Piston	1	0	0	1
Horizontal tilt	2	1	1	$2r\cos(\theta)/\sqrt{1+\varepsilon^2}$
Vertical tilt	3	1	−1	$2r\sin(\theta)/\sqrt{1+\varepsilon^2}$
Defocus	4	2	0	$\sqrt{3}(1+\varepsilon^2-2r^2)/(\varepsilon^2-1)$
Oblique astigmatism (45 deg)	5	2	−2	$\sqrt{6}r^2\sin(2\theta)/\sqrt{1+\varepsilon^2+\varepsilon^4}$
Astigmatism (0 deg)	6	2	2	$\sqrt{6}r^2\cos(2\theta)/\sqrt{1+\varepsilon^2+\varepsilon^4}$
Vertical coma	7	3	−1	$\frac{2\sqrt{2}r(-2-2\varepsilon^4+3r^2+\varepsilon^2(-2+3r^2))\sin(\theta)}{\sqrt{(\varepsilon^2-1)^2(1+\varepsilon^2)(1+4\varepsilon^2+\varepsilon^4)}}$
Horizontal coma	8	3	1	$\frac{2\sqrt{2}r(-2-2\varepsilon^4+3r^2+\varepsilon^2(-2+3r^2))\cos(\theta)}{\sqrt{(\varepsilon^2-1)^2(1+\varepsilon^2)(1+4\varepsilon^2+\varepsilon^4)}}$
Oblique trefoil (0 deg)	9	3	−3	$2\sqrt{2}r^3\sin(3\theta)/\sqrt{1+\varepsilon^2+\varepsilon^4+\varepsilon^6}$
Horizontal trefoil (30 deg)	10	3	3	$2\sqrt{2}r^3\cos(3\theta)/\sqrt{1+\varepsilon^2+\varepsilon^4+\varepsilon^6}$
Spherical aberration	11	4	0	$\sqrt{5}(1+\varepsilon^4-6r^2+6r^4+\varepsilon^2(4-6^2))/(\varepsilon^2-1)^2$

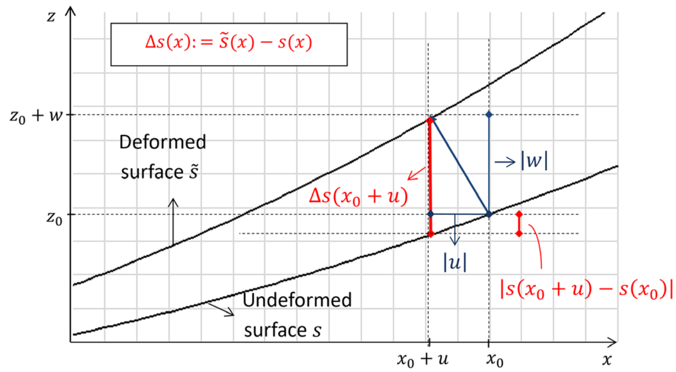

Fig. 5 Derivation (2D) of the mirror sag change at the displaced node in terms of finite-element displacements.

The second term on the right side of the equation above is simply the difference of the base surface evaluated at the displaced node and the undeformed node. In the calculations of the optical aberrations, we utilized Eq. (12), which provides the deformation of the sag at the displaced node, as an alternative to Eq. (11), which approximates the sag deformation at the undeformed node. In the calculations of the optical aberrations, we fitted Eq. (12) into the annular Zernike polynomials and solved for the coefficients by the least-squares method in MATLAB. Finally, we imported the obtained Zernike coefficients into Zemax and compared the optical performances of the two beam director systems, the primary mirrors of which are made of borosilicate and Zerodur®, respectively.

3 Numerical Results and Discussion

3.1 *Temperature Distribution and Deformation*

2D electromagnetic analysis was performed in COMSOL®, and it was concluded that with the given reflective coating the reflection rate of the laser at the study frequency is 99.9706%. This means that 0.0281% of the electromagnetic energy was dissipated as thermal energy inside the mirror domain. More than 50% of this thermal energy was already absorbed within the first pair of layers, 76% within the second pair, and 99% within the seventh pair, which corresponded to only 2 μm of thickness (Fig. 6). These results suggest that the laser beams in the thermomechanical models can be treated as surface heat sources with an absorptivity of $A = 0.03\%$.

In the second part of the FEA study, the temperature distribution and the deformation of the mirror surface in all three dimensions due to the laser heating was computed. First, a steady-state analysis was performed without the laser heating to calculate the gravity only deformation of the surface. Then a time-dependent thermomechanical analysis involving the laser heating was carried out for the first 30 s, with the laser source power taken to be 6×4 kW and the absorptivity of the mirror surface to be $A = 0.03\%$. This scenario suggested that, out of 4 kW heat power deposited on the mirror surface per beam, only 1.2 W was absorbed. Each beam was considered to have a Gaussian spot size of 47 mm, which resulted in an effective surface heat source with a peak irradiance of $0.346\ \mathrm{kW/m^2}$ per beam. All of the analyses were performed for both borosilicate and Zerodur substrate materials. The ambient and reference temperatures were set to 20°C.

To investigate other cases such as a different coating or utilization of a higher power laser source, we also performed analyses with different absorbed powers while keeping the beam spot size the same for all cases. Therefore, we considered the cases with the mirror absorbing 1.2, 2, 4, and 6 W per beam. These values are the total absorbed power and may either imply a high-power laser versus a good coating or vice versa.

According to the results, the effect of gravity on the deformation of the mirror surface is similar for both substrate materials, with borosilicate having a slightly larger deformation. In this case, maximum sag displacements calculated on the front surfaces were 3.6 nm for

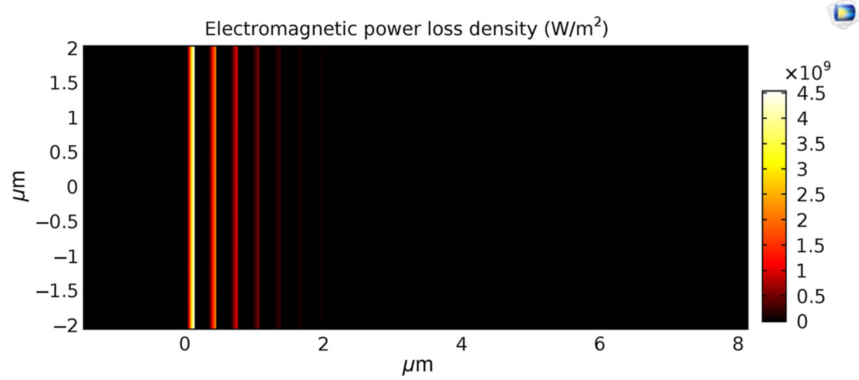

Fig. 6 Electromagnetic analysis: the heat dissipation through the coating layers. The calculated absorptivity $A = 0.0281\%$, reflectance $R = 99.9706\%$, and transmittance $T = 0.0013\%$. Out of the total dissipated energy, 99% was absorbed within the first seven pairs of layers (2 μm).

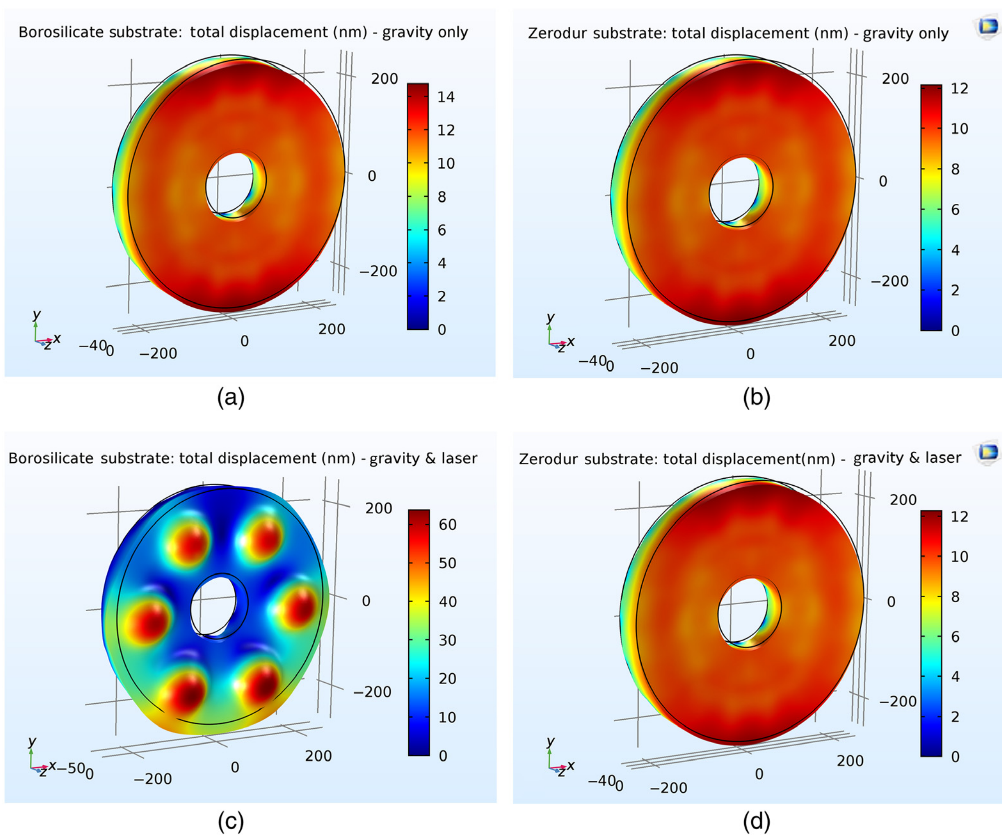

Fig. 7 Thermomechanical analysis: total displacements (in nm) of the mirror surfaces: (a), (b) with no laser heating/gravity only and (c), (d) with laser heating; (a), (c) for borosilicate substrate on the left and (b), (d) Zerodur substrate on the right. Total laser power absorbed by both mirrors is $\mathrm{Pa} = 6 \times 1.2$ W for 30 s. Deformations exaggerated by a factor of 7×10^5.

Zerodur® and 4.5 nm for borosilicate substrates. When we consider laser heating with absorbed powers from 1.2 up to 6 W per beam, the maximum temperature changes on the mirror surfaces were also similar for both materials and <7°C after 30 s of exposure for all cases (Fig. 8).

However, since borosilicate has a higher thermal expansion coefficient compared with that of Zerodur®, deformations of the surfaces due to laser heating were quite different when the two substrate materials were compared. For all cases after 30 s, the maximum sag displacements for

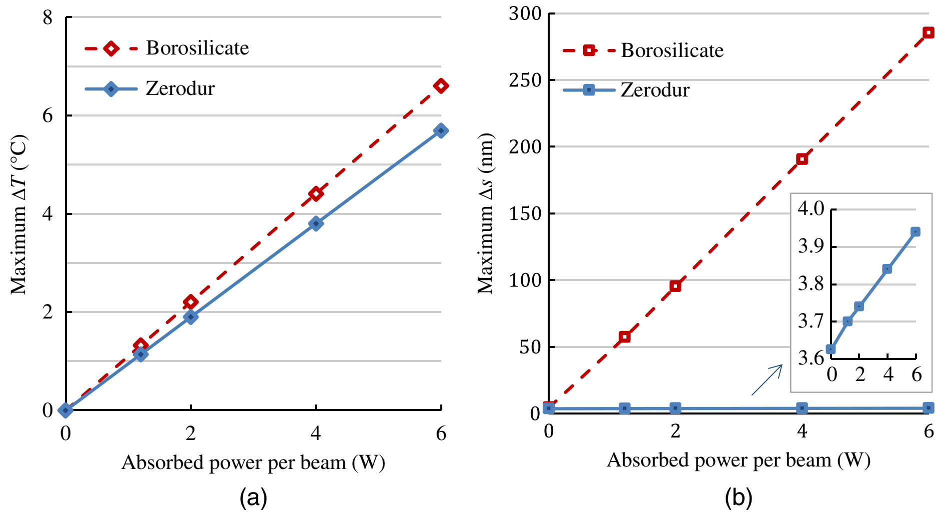

Fig. 8 (a) Maximum temperature changes ΔT(°C) and (b) maximum sag displacements $\Delta s_{\max}$ (nm) calculated on the front surfaces of the mirrors at 30 s versus the amount of power absorbed by the mirrors per beam.

the Zerodur® substrate stayed around 4 nm; for the borosilicate substrate on the other hand, they reached values ranging from 57 to 285 nm. In other words, when exposed to the laser heating for a short period of time, Zerodur® experiences a deformation increasing with the absorbed laser power but for all cases only slightly larger than the one due to gravity whereas borosilicate showed a significant deformation compared with the effect of gravity and kept increasing linearly with the absorbed power (Figs. 7 and 8).

In addition to the peak deformation values, we also studied the displacement slopes to analyze the effect of the deformation on the surface topology. As seen in Fig. 9, the average z-displacement gradients of the mirror surface increase linearly with the increasing absorbed power for both materials. Yet, the increase for the borosilicate substrate was approximately 10 times steeper compared with that of Zerodur.

3.2 *Zernike Coefficients, RMS Wavefront Error, Spot Size, and MTF*

To fully understand how deformation due to gravity and laser heating combined affect the optical performance, we calculated Zernike annular coefficients of the deformed surfaces in MATLAB and compared the two substrate materials. RMS wavefront errors (W_{RMS}) were computed for the deformed mirror surfaces before and after laser exposures of 30 s. In these calculations, the mechanical alignment error was not considered, and the wavefront piston was subtracted out from the RMS wavefront error, which is expressed in units of laser wavelength λ (1075 nm).

When we consider the mechanical load due only to gravity (without laser heating), borosilicate and Zerodur® exhibit a similar behavior, with RMS wavefront errors of both being less

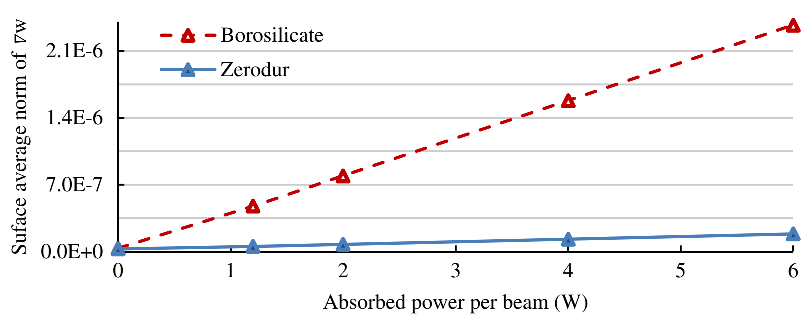

Fig. 9 Average z-displacement gradients $\frac{1}{A}\iint_A \|\nabla w\| dS$ calculated on the two mirror surfaces after 30 s of laser exposure versus the amount of power absorbed by the mirrors per beam.

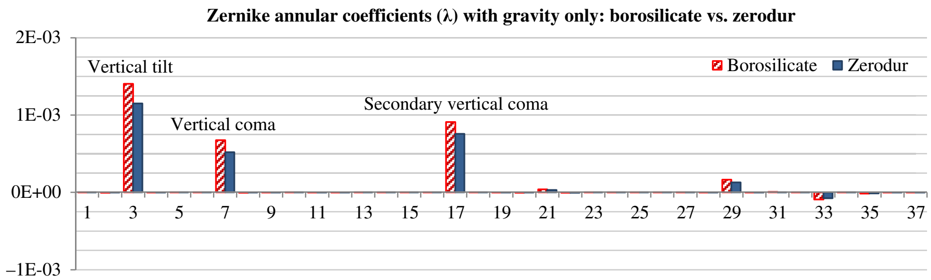

(a)

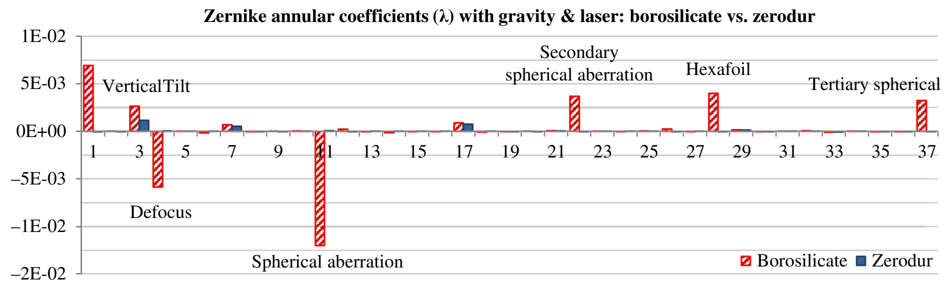

(b)

Fig. 10 Comparison of Zernike phase coefficients for borosilicate and Zerodur® substrates with (a) gravity only and (b) after 30 s of laser exposure with absorbed power of 1.2 W per beam. Coefficients are in units of laser wavelength.

than 2.0×10^{-3} wave. Vertical coma and vertical tilt were the dominant aberrations (see Fig. 10) due to the conical shapes of the mirror surfaces and the asymmetry caused by the gravitational force applied in the vertical direction. (Utilizing a hyperbolic secondary mirror in the telescope system will help to reduce this coma.) We, on the other hand, benefited from having conical surfaces for the sake of which spherical aberrations are eliminated.

When we added a thermal load with laser heating, in the case of the Zerodur® substrate, defocus and spherical aberrations came into play due to the deformation of the surface, and they grew with the increasing absorbed powers, but much less than the previously obtained vertical tilt and coma (see Fig. 11). RMS wavefront errors for all cases remained under 2.0×10^{-3} wave for Zerodur (more precisely, under 1.6×10^{-3} wave).

When the laser heating was applied to the borosilicate, deformation due to the thermal expansion caused the defocus and the spherical aberrations to dominate together with the hexafoil, all of which increased with the increasing absorbed power. The reason that the hexafoil showed up here is the six-beam configuration causing six bumps on the mirror surface and on the outcoming wavefront accordingly. The RMS wavefront error also increased linearly with the absorbed power, starting with 1.5×10^{-2} wave for an absorbed power of 6×1.2 W and reaching 7.4×10^{-2} wave for an absorbed power 6×6 W, which still remained nearly at the diffraction-limited level.

In the next step, the calculated Zernike coefficients for the primary mirror were implemented into Zemax, and the optical performances of the telescope system were analyzed. The MTF analyses were performed and the laser beam spot sizes were computed in Zemax for all of the absorbed power cases via physical optics modeling. Spot sizes calculated here are the maximum of the laser beam radii ($1/e^2$) of all (six) beams evaluated at the target at which the laser beams are directed. Here imaging performance was evaluated at a 800 nm wavelength since appropriate optics (e.g., dichroic mirrors and bandpass filters) in a typical beam director system with a shared aperture for simultaneous use of a high power and an imaging laser uses a monochromatic imaging at 800 nm. The optical components of the beam director system in this work were all assumed to be fabricated and aligned with diffraction limited tolerances. The secondary mirror was also assumed to be free of aberrations in these analyses.

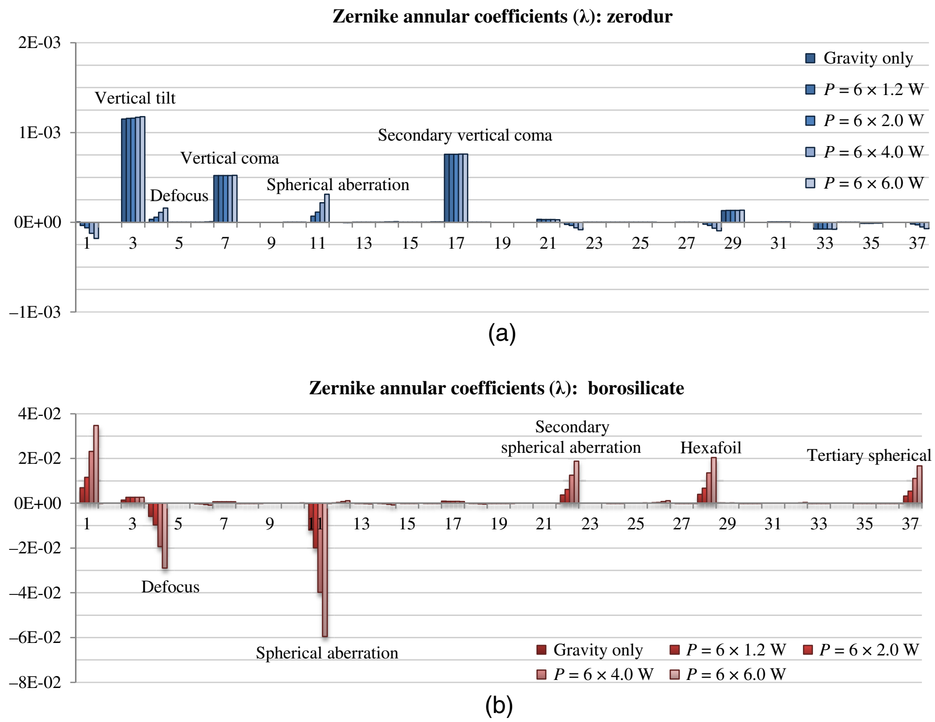

Fig. 11 Zernike phase coefficients calculated for the deformed mirror surfaces for both (a) Zerodur® and (b) borosilicate substrates. Comparative results with gravity only and after 30 s of laser exposure with absorbed powers from 1.2 to 6 W per beam. Zernike coefficients are in units of laser wavelength.

According to the results, diffraction limited airy disk has a radius of 7.4 mm for both Zerodur® and borosilicate substrates. The spot diagrams and the MTF graphs are identical for both substrates and the RMS spot radius stays within the airy disk when no laser is applied (only gravitational load is taken into account).

When the Zerodur® mirror was exposed for 30 s, only a negligible change could be observed in the spot size or on the MTF graphs for any absorbed power up to 6 W per beam. However, for the borosilicate mirror, the effect of the laser heating at six spots can be seen in the spot diagrams even in the smallest absorbed power case (6×1.2 W), though the RMS spot size is still smaller than the airy disk, resulting in insignificant performance degradation. When the absorbed power reaches 6 W per beam, the RMS spot size starts to exceed along with degradation in the airy disk size and the MTF as shown in Figs. 12 and 13. The effect of the change in the wavefront error shows itself in the Strehl ratio values, which decrease as the absorbed laser power increases as shown in Table 3. Therefore, from these values we can assert that, for all but the 6 W absorbed power case, the system can be considered to be diffraction limited. We believe that under 6 W absorbed power per beam, these error levels are promising for directed beam applications in which the spot size is the most central factor for casting the necessary energy intensity on the target. Also note that, in this work, we focused only on laser-induced aberrations and their implications on the laser focusing and imaging performance of the beam director; atmospheric effects (i.e., absorption, scintillations, and thermal blooming) and tracking errors have not been included.

It is worth pointing out that primary mirror size is generally determined by the number of laser sources and their beam sizes. And laser output beam sizes are optimized for the power handling level of the coating, diffraction, and atmospheric effects. Therefore, using a larger primary mirror may enable utilization of larger laser beam sizes and in turn, reduced wavefront distortion because of low-power intensity on the mirror. On the other hand, larger mirrors with high-quality coatings are difficult and costly to fabricate. Moreover, larger mirrors result in heavier and bulkier telescopes with increased gravitational wavefront distortion in addition to requirements of costly mechanic controls and alignment systems.

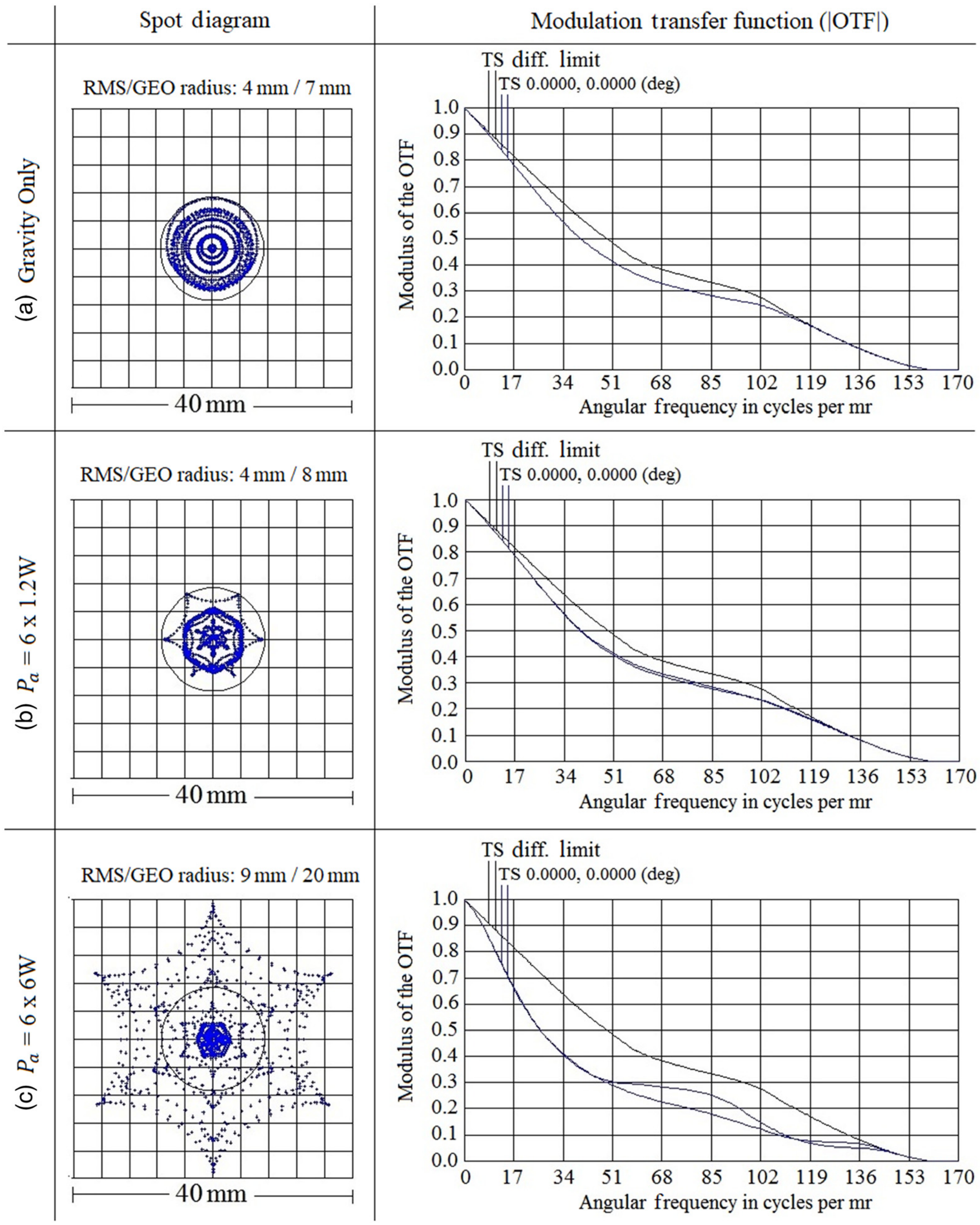

Fig. 12 Spot diagrams (left) and MTF (right) graphs for borosilicate substrate mirror. Results are presented for three different cases: the effect(s) of (a) gravity only (no laser); (b) gravity and laser heating with 1.2 W power absorbed per beam; and (c) gravity and laser heating with 6 W power absorbed per beam. Duration of laser heating is 30 s.

4 Conclusion

In the present work, an extensive mathematical model for computing the optical aberrations caused by high-power laser induced conformal conical mirror surface deformations is presented. Surface deformations in all three dimensions due to the laser exposure together with gravity were computed in a time-dependent FEA. Laser- and gravity-induced optical aberrations caused by the surface deformations were analyzed by means of Zernike polynomials. The deformed surface sag calculated in the thermomechanical analysis was fitted into Zernike polynomials and coefficients were computed in MATLAB by the least squares method. Laser-induced aberrations as well as their effects on the beam director performance were analyzed for two exemplary primary conical telescope mirrors with borosilicate and Zerodur© substrates. High-power laser spot size

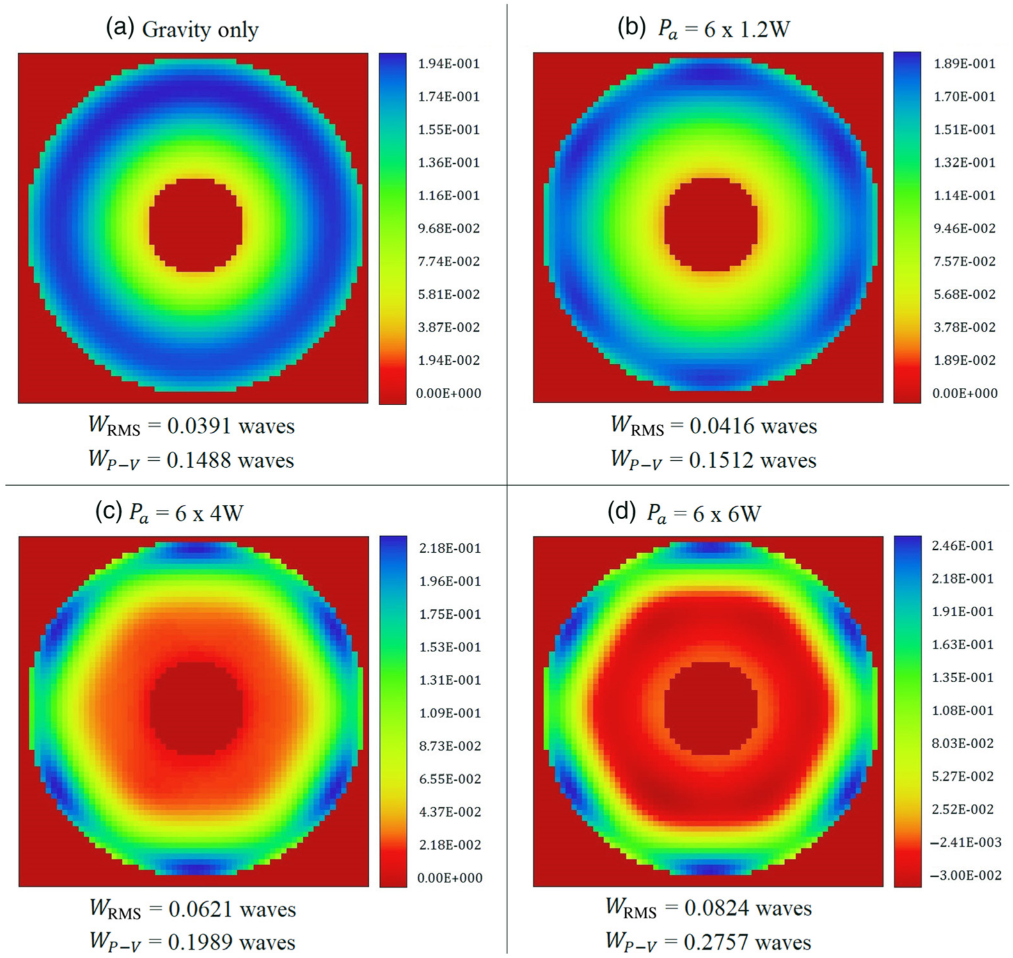

Fig. 13 Wavefront functions at 800 nm for borosilicate substrate mirror. Results are presented for four different cases: the effect(s) of (a) gravity only (no laser) and (b)–(d) gravity and laser heating with 1.2,4,6 W power absorbed per beam, respectively. Duration of laser heating is 30 s. Laser and imaging wavelengths are 1075 and 800 nm, respectively.

Table 3 RMS wavefront errors of the deformed primary mirror itself (M1) under the load of gravity, the thermal expansion due to laser heating for 30 s, and the resulting errors of the telescope system.

	Borosilicate substrate				Zerodur substrate			
	M1	Telescope system			M1	Telescope system		
Absorbed power per beam by M1	W_{RMS} (wave)	W_{RMS} (wave)	Strehl ratio	Laser beam spot size (mm)	W_{RMS} (wave)	W_{RMS} (wave)	Strehl ratio	Laser beam spot size (mm)
Gravity (W)	1.82×10^{-3}	3.91×10^{-2}	0.94	3.75	1.48×10^{-3}	3.91×10^{-2}	0.94	3.75
1.2	1.51×10^{-2}	4.16×10^{-2}	0.93	4.54	1.49×10^{-3}	3.91×10^{-2}	0.94	3.75
2.0	2.48×10^{-2}	4.58×10^{-2}	0.92	5.35	1.50×10^{-3}	3.91×10^{-2}	0.94	3.75
4.0	4.93×10^{-2}	6.21×10^{-2}	0.86	7.79	1.52×10^{-3}	3.91×10^{-2}	0.94	3.75
6.0	7.38×10^{-2}	8.24×10^{-2}	0.76	10.49	1.55×10^{-3}	3.91×10^{-2}	0.94	3.75

and MTF were analyzed in detail via computing the respective coefficients of the Zernike polynomials under various laser exposures together with the effect of gravity.

According to the performed analyses, the Zerodur substrate deformed only slightly under various laser (thermal) loads that yielded vertical tilt and coma aberrations with relatively negligible amplitudes on the order of 1×10^{-3} wave (Zernike polynomials 3rd, 7th, 17th). A beam director system with such a primary mirror showed diffraction limited performance regardless of the laser power owing to the low-thermal expansion properties of the Zerodur material.

On the other hand, the borosilicate mirror yielded a similar deformation and aberrations without laser exposure, yet experienced greater deformations leading to predominantly spherical and defocus aberrations (Zernike polynomials 4th, 11th), which vary linearly with laser power and have relatively larger amplitudes (i.e., on the order of 1×10^{-2} wave). Therefore, it can be deduced that high-power laser-induced aberrations with typical high thermal expansion materials are mainly spherical and defocused. However, optical performance of a beam director system with a primary mirror having a borosilicate substrate will not suffer too much. For all cases analyzed in this work, the borosilicate substrate led to at most twice the wavefront error amplitude (i.e., 8.24×10^{-2} wave) as that of the Zerodur (i.e., 3.91×10^{-2} wave) for the telescope system, and the system performance was comparable (diffraction limited) for both substrates under 6 W laser power absorption (per beam). Thus a borosilicate mirror may be utilized in such laser systems under certain ambient temperatures as long as a high-performance coating is accessible to reduce the total laser absorption. This will allow one to take advantage of the cost-effectiveness, easily manufacturability, and light weight of borosilicate materials for laser beam director applications.

5 Appendix A. Zernike Coefficient and Name List in Zemax Order

Zernike polynomial coefficients presented in Figs. 10 and 11 and corresponding aberration names are listed in Table 4 as in the order listed in Zemax.

Table 4 Primary, secondary, and tertiary Zernike coefficients and name list in Zemax order.

#	*n*	*m*	Aberration name	#	*n*	*m*	Aberration name
1	0	0	Piston	22	6	0	Secondary spherical
2	1	1	Horizontal tilt (tip)	23	6	−2	Tertiary oblique astigmatism (45 deg)
3	1	−1	Vertical tilt	24	6	2	Tertiary (vertical) astigmatism (0 deg)
4	2	0	Defocus	25	6	−4	Secondary oblique tetrafoil
5	2	−2	Oblique astigmatism (45 deg)	26	6	4	Secondary vertical tetrafoil
6	2	2	(Vertical) astigmatism (0 deg)	27	6	−6	Oblique hexafoil
7	3	−1	Vertical coma	28	6	6	Vertical hexafoil
8	3	1	Horizontal coma	29	7	−1	Tertiary vertical coma
9	3	−3	(Vertical) trefoil (0 deg)	30	7	1	Tertiary horizontal coma
10	3	3	Oblique trefoil (30 deg)	31	7	−3	Tertiary (vertical) trefoil (0 deg)
11	4	0	Spherical	32	7	3	Tertiary oblique trefoil (30 deg)
12	4	2	Secondary astigmatism (0 deg)	33	7	−5	Secondary vertical pentafoil
13	4	−2	Secondary oblique astigmatism (45 deg)	34	7	5	Secondary oblique pentafoil
14	4	4	Vertical tetrafoil	35	7	−7	Vertical heptafoil

Table 4 (*Continued*).

#	*n*	*m*	Aberration name	#	*n*	*m*	Aberration name
15	4	−4	Oblique tetrafoil	36	7	7	Oblique heptafoil
16	5	1	Secondary horizontal coma	37	8	0	Tertiary spherical
17	5	−1	Secondary vertical coma				
18	5	3	Secondary oblique trefoil (30 deg)				
19	5	−3	Secondary (vertical) trefoil (0 deg)				
20	5	5	Oblique pentafoil				
21	5	−5	Vertical pentafoil				

References

1. D. Petring et al., "The relevance of brightness for high power laser cutting and welding," in *Int. Congr. Appl. Lasers Electro-Opt.*, p. 206 (2008).
2. J. Canning, "Fibre lasers and related technologies," *Opt. Lasers Eng.* **44**(7), 647–676 (2006).
3. C. Kopp, "High energy laser directed energy weapons" (2014).
4. Y. Michine and H. Yoneda, "Ultra high damage threshold optics for high power lasers," *Commun. Phys.* **3**, 24 (2020).
5. T. Tolenis et al., "Next generation highly resistant mirrors featuring all-silica layers," *Sci. Rep.* **7**, 10898 (2017).
6. D. S. Hobbs and B. D. MacLeod, "High laser damage threshold surface relief micro-structures for anti-reflection applications," *Proc. SPIE* **6720**, 67200L (2007).
7. T. I. Suratwala et al., "HF-based etching processes for improving laser damage resistance of fused silica optical surfaces," *J. Am. Ceram. Soc.* **94**(2), 416–428 (2011).
8. T. Tolenis et al., "Sculptured anti-reflection coatings for high power lasers," *Opt. Mater. Express* **7**(4), 1249–1258 (2017).
9. P. Hello and J. Y. Vinet, "Analytical models of thermal aberrations in massive mirrors heated by high power laser beams," *J. Phys. Paris* **51**, 1267–1282 (1990).
10. P. Kwee et al., "Stabilized high-power laser system for the gravitational wave detector advanced LIGO," *Opt. Express* **20**(10), 10617–10634 (2012).
11. C. Bogan et al., "Novel technique for thermal lens measurement in commonly used optical components," *Opt. Express* **23**(12), 15380–9 (2015).
12. G. M. Harry, "Advanced LIGO: the next generation of gravitational wave detectors," *Class. Quantum Gravity* **27**, 084006 (2010).
13. L. Yang, Z. Wu, and B. Zhang, "Influence of thermal deformation of a multilayer dielectric grating on a spectrally combined beam," *Appl. Opt.* **55**(32), 9091–9100 (2016).
14. H. Wang et al., "Simulation and experimental study of laser-induced thermal deformation of spectral beam combination grating," *Opt. Express* **28**(22), 33334–33345 (2020).
15. M. R. Kozlowski et al., "High-power optical coatings for a megajoule-class ICF laser," *Proc. SPIE* **1782**, 105 (1993).
16. I. MacMillan, "Creating high-power optical coatings is complex," *Laser Focus World* **38**(5), 137–144 (2002).
17. L. Hornsby, R. C. Hopkins, and H. P. Stahl, "Thermal analysis of the advanced technology large aperture space telescope (ATLAST) 8-meter primary mirror," *Proc. SPIE* **7731**, 77312R (2010).
18. R. Volkmer et al., "Optical and thermal design of the main optic of the solar telescope GREGOR," *Proc. SPIE* **5179**, 270 (2003).
19. Schott, "ZERODUR® zero expansion glass ceramic catalogue," (2011).
20. Schott, "BOROFLOAT® 33—thermal properties datasheet," (2018).

21. Schott, "BOROFLOAT® 33—mechanical properties datasheet," (2018).
22. J. Han et al., "The characteristics of Ta_2O_5 films deposited by radio frequency pure oxygen ion assisted deposition (RFOIAD) technology," *J. Appl. Phys.* **121**(6), 65302 (2017).
23. R. Chandrasekharan et al., "Change in radiative optical properties of Ta_2O_5 thin films due to high-temperature heat treatment," *J. Heat Transfer* **129**(1), 27–36 (2007).
24. R. Kitamura, L. Pilon, and M. Jonasz, "Optical constants of silica glass from extreme ultraviolet to far infrared at near room temperature," *Appl. Opt.* **46**(33), 8118–8133 (2007).
25. H. Kaushal et al., "Experimental investigation of optimum beam size for FSO uplink," *Opt. Commun.* **400**, 106–114 (2017).
26. S. J. Park et al., "Design of primary mirror for laser beam director," *Proc. SPIE* **6034**, 60340F (2006).
27. V. V Skorokhod, "Layered composites: structural classification, thermophysical and mechanical properties," *Powder Metall. Met. Ceram.* **42**(9), 437–446 (2003).
28. B. Liu, X. Feng, and S.-M. Zhang, "The effective Young's modulus of composites beyond the Voigt estimation due to the Poisson effect," *Compos. Sci. Technol.* **69**(13), 2198–2204 (2009).
29. D. R. M. Crooks et al., "Experimental measurements of mechanical dissipation associated with dielectric coatings formed using SiO_2, Ta_2O_5 and Al_2O_3," *Class. Quantum Gravity* **23**(15), 4953–4965 (2006).
30. P. A. Baisden et al., "Large optics for the national ignition facility," *Fusion Sci. Technol.* **69**(1), 295–351 (2016).
31. V. N. Mahajan, "Zernike annular polynomials for imaging systems with annular pupils," *J. Opt. Soc. Am.* **71**(1), 75–85 (1981).
32. K. B. Doyle, V. L. Genberg, and G. J. Michels, *Integrated Optomechanical Analysis*, 2nd ed., SPIE Press, Bellingham, Washington (2002).

Emine Yasemen Kaya Cekin received her BSc degree in mathematics from Bilkent University, Bilkent, Turkey, in 2006 and her PhD in applied mathematics from Texas Tech University, Lubbock, Texas, USA, in 2011. She is a senior researcher at the Electro-Optic and Lasers Systems Group at TUBITAK (The Scientific and Technological Research Council of Turkey). Her current research interests include mathematical modeling and simulation of laser-material interactions, optical aberrations, and optomechanical systems.

Yavuz Ozturk received his BSc and MSc degrees in physics from Bilkent University, Turkey, in 2002 and 2004. He received his PhD in physics from Gebze Technical University in 2017. He was a member of the Electro-Optic and Lasers Systems Group at TUBITAK from 2013 to 2019, where he focused on optomechanical and laser system analysis. He is currently with the electrical engineering division of the University of Cambridge and working on HTS MRI magnets.

Eray Arpa received his BSc degree in physics from the Middle East Technical University, Ankara, Turkey, in 2014 and his MSc degree in physics from Gebze Technical University, Gebze, Turkey, in 2020. He worked in the Laser and Electro-Optical Systems Group at TUBITAK from 2015 to 2020. He is a senior researcher at the Space Technologies Research Institute of TUBITAK. His current research interests include optical design, optomechanical design, and optical alignment and metrology.

Aydın Yeniay received his BS degree in engineering physics from Ankara University, Ankara, Turkey, and his MSc degree and PhD in physics from Lehigh University, Bethlehem, Pennsylvania, USA, in 1996 and 2000, respectively. He is an assistant professor in the Electro-optic and Lasers Systems Group at TUBITAK. He is the author of more than 20 publications and holds more than 10 patents. His current research interests include high-power laser systems, fiber lasers/amplifiers, nonlinear fiber optics, and optical communications.